

Transverse Strain Aging Behaviour of Uncoated Thick Walled X70 UOE Microalloyed Steel Pipes

J.B. Wiskel, J. Ma, D.G. Ivey and H. Henein

Dept. of Chemical and Materials Engineering
University of Alberta
Edmonton, Alberta, Canada T6G 1H9

ABSTRACT

Transverse tensile samples were extracted from the centreline position of three different compositions of uncoated thick walled microalloyed X70 UOE pipe at a location 180° from the weld. Aging heat treatments of 5, 15, and 25 minutes and temperatures of 175, 215, and 255°C were applied. Tensile tests were conducted on both the original pipe and on pre-strained samples. Microstructural analysis was undertaken using optical microscopy and scanning electron microscopy (SEM). The effects of a combined time and temperature aging parameter, pre-strain, microstructure and tensile work hardening behaviour on the pipe yield stress and yield to tensile strength ratio, is presented.

INTRODUCTION

Strain aging of microalloyed pipe steel – resulting in a change in yield stress ($\Delta\sigma_y$) and/or a change in the yield to tensile strength ratio ($\Delta Y/TS$) – can be important in coated pipe, pipe exposed to slightly elevated temperature (e.g., direct exposure to the sun during storage) or for pipe at relatively low temperature but in service for long periods of time. The strain aging phenomenon is attributed to the diffusion to and interaction of carbon (and/or nitrogen) with mobile dislocations present in the microstructure. This interaction effectively “pins” the dislocations and potentially alters the mechanical properties. Important parameters in the strain aging process are time and temperature (for carbon diffusion) and microstructure via its effect on mobile dislocation distribution and/or density.

In general, it is difficult to quantify the mobile dislocation distribution/density by direct measurement. Therefore, an indirect assessment of mobile dislocation density is made by quantifying the work hardening behaviour of the as-received

(non-aged) pipe steel and relating this parameter to strain aging behaviour. In addition, the effect on microstructure on strain aging will also be analyzed.

The work presented in this paper quantifies the effect of aging time and temperature, pre-strain, microstructure and tensile work hardening behaviour on the change to both the yield stress ($\Delta\sigma_y$) and the yield/tensile strength ratio ($\Delta Y/TS$) for three (3) types (i.e., different microstructures and C/Nb ratios) of uncoated UOE X70 pipe steel. The tensile samples tested were taken at a position 180° to the weld and in the transverse direction. Longitudinal tensile samples were also taken at the same location (relative to the weld). This work is a continuation of research conducted by the authors [1] on the effect of strain aging on longitudinal tensile properties at a location 90° to the weld.

BACKGROUND

Numerous studies have been published (an overview of these studies can be found in Wiskel et al. [1]) on both the mechanism of strain aging and on strain aging of microalloyed steels used in pipelines. However, as stated earlier, an objective of the work presented is to assess how the as-received work hardening behaviour of the pipe steel affects its susceptibility to strain aging. Thus, before proceeding with a description of the strain aging testing and subsequent analysis, a review of the literature on work hardening behaviour of metals during the initial stages of plastic deformation during tensile testing is presented.

Microalloyed steels can also experience the Bauschinger Effect (B.E.) when subjected to complex forming conditions (e.g., tension/compression strain reversals) such as what may occur during the UOE forming process and/or during flattening of tensile specimens. As the tensile bars in this work are

machined, the flattening effect is negated. The Chaboche kinematic model, used to quantify the B.E. during initial stages of tensile testing, will be reviewed.

Work Hardening

A well known empirical relationship to describe the stress-strain behaviour of metals is the Holloman equation [2]:

$$\sigma = K \cdot \varepsilon^n \quad (1)$$

where K is a material constant, ε is the true strain and n is the strain hardening index or coefficient. The value of n can be used to assess the work hardening behaviour of different material and/or microstructures. However, the application of this equation to an entire stress-strain curve must be treated with caution as firstly, the value of n can vary with strain and secondly, the stress strain curve must show continuous yielding. The analysis presented in this work determined n as function of strain along the continuous stress-strain curve.

The rate of work hardening during deformation can be determined from the value of n using [2]:

$$\frac{d\sigma}{d\varepsilon} = \frac{n \cdot \sigma}{\varepsilon} \quad (2)$$

Bergstrom [3] developed a model for describing work hardening as a function of strain. Included in the model are terms for the generation, annihilation, immobilization and remobilization of dislocation during straining. This model illustrates that the work hardening rate at any particular strain is a function of dislocation behaviour. In the context of the work presented in this paper, a variation in the work hardening rate measured for the as-received material may provide a semi-quantitative measure of steel's susceptibility to strain aging.

Bauschinger Effect

The initial part of a stress-strain curve taken from a pipe sample can be significantly different from that taken from the initial skelp material due to the Bauschinger effect. Depending on the strain history incurred in the pipe forming process, the initial portion of a tensile stress-strain curve can be highly non-linear [4]. The nonlinearity in stress/strain behaviour observed in the transverse tensile tests conducted in this work can be described mathematically by the following kinematic hardening equation:

$$\dot{\alpha} = C \frac{1}{\sigma^o} (\sigma - \alpha) \cdot \dot{\varepsilon}^{pl} - \gamma \cdot \alpha \cdot \dot{\varepsilon}^{pl} \quad (3)$$

where α is the current position of the elastic domain is stress, $\dot{\alpha}$ is the rate of change in α in stress space, σ is the stress tensor, σ^o is the size of the elastic domain, C is the initial kinematic hardening modulus, γ determines the rate at which the kinematic hardening modulus decreases and $\dot{\varepsilon}^{pl}$ is the equivalent plastic strain rate. A C/γ ratio are will be used to compare the kinematic hardening effect of three steels studied in this work. With increasing amount of plastic strain (during

the tensile test) the value of $\dot{\alpha}$ approaches zero (0) and isotropic hardening dominates. At this stage in the test, Equation (2) can be applied to determine the work hardening rate of the steel being tested.

EXPERIMENTAL PROCEDURE AND RESULTS

Three (3) different, thick walled, X70 UOE pipes were examined in this work. Table 1 summarizes the UOE pipe steel characteristics including the wall thickness (t), the wt% of Mn, N and Ti and the C/Nb ratio. The principle composition difference between all three steels is the C/Nb ratio. For proprietary reasons, the full composition is not given. Soluble nitrogen (N) can contribute to the strain aging effect, however, the level of Ti present in the steels is deemed sufficient to diminish this effect. Specific thermomechanical controlled processing (TMCP) parameters from the pipes studied were not available.. All three UOE pipes were 914 mm in diameter and were received in the uncoated condition.

Table 1 - UOE pipe steel specifications

Steel	t (mm)	Mn (wt%)	N (ppm)	Ti (wt%)	C/Nb ratio
A	19.1	1.60	40	0.014	0.6
B	19.0	1.65	40	0.013	1.2
C	20.4	1.59	<40	0.017	1.8

Tensile Testing – As Received Pipe Material

Cylindrical tensile bars were taken at a position 180° from the UOE weld and transverse to the pipe length. Due to the curvature of the pipe, and the need to have a suitable sample length, a tensile bar could only be machined from a region encompassing the centre line of the pipe (see Figure 1 below).

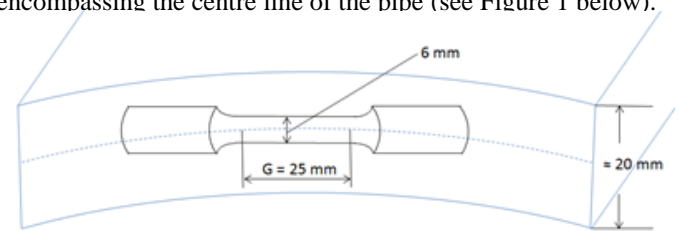


Figure 1 - Transverse tensile sample

The stress strain graph for the initial part of the tensile test for sample A2-A29-AR (as-received condition for Steel A) is shown in Figure 2. Included in Figure 2 is the 0.5% offset yield strength value of 567 MPa, an initial linear elastic region, a “round house” region (between $\approx 0.12\%$ and 0.5% strain) in which behaviour is attributed primarily to kinematic hardening (i.e., the Bauschinger effect) and a region beginning at approximately 0.5% that corresponds to isotropic hardening behaviour only. The transverse tensile test curves studied in this work all exhibited a similar shape to that shown in Figure 2.

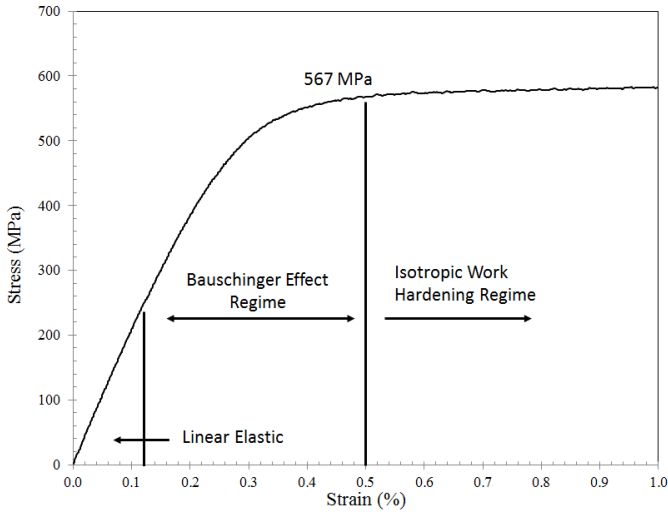


Figure 2 - Tensile curve for A2-A29-AR

Initial Work Hardening Rate and Bauschinger Effect

From the isotropic work hardening regime, a local strain hardening coefficient (n) value was obtained from the slope of the $\ln(\sigma)$ vs. $\ln(\epsilon)$ curve using a moving average (in 0.5% strain increments) regression analysis methodology. The value of stress and the value of strain at the midpoint of each strain increment, along with local value of n , were incorporated into Equation 2 to obtain the local work hardening rate. In addition, the C/γ ratio (Equation 3) for each tensile test were obtained from the Bauschinger effect regime using techniques developed in a previous work by the authors [4]. The yield stress (σ_y), the ultimate tensile stress (TS), the initial strain hardening rate ($d\sigma/d\epsilon$) and the value of the C/γ ratio determined for all three as-received pipe steels are tabulated in Table 2.

Table 2 – As-received transverse tensile test data

Sample Designation	σ_y (MPa)	TS (MPa)	$d\sigma/d\epsilon$ (MPa/%)	C/γ
A2-A13-Pre	570	-	3105	316
A2-A20-Pre	565	-	2977	341
A2-A24-Pre	565	-	3078	303
A2-A29	567	657	3093	305
B2-B5-Pre	523	-	5125	287
B2-B11-Pre	530	-	4694	272
B2-B16-Pre	522	-	4997	245
B2-B24-Pre	516	-	5659	262
B2-B18	524	638	4713	263
C2-C2-Pre	555	-	2972	264
C2-C3-Pre	540	-	3404	308
C2-C8-Pre	555	-	3253	271
C2-C5	574	665	3302*	-

* Work hardening following discontinuous yielding

Only a select number of the as-received or pre-strained tensile tests are shown in Table 2 as many of the samples exhibited similar tensile behaviour. In addition, the tensile strength (TS) was not obtained for samples that were pre-strained to either 1.5% or 3.0%; these samples are defined with the “Pre” suffix.

On examination of Table 2, it is observed that Steel B exhibits a higher initial work hardening rate (> 4700) than either Steel A (≈ 3050) or Steel C (≈ 3300). Alternately, Steel B exhibit a slightly lower C/γ ratio (average = 268) versus Steel A (average = 316). These differences in the work hardening rates and C/γ ratios may be attributed to a possible difference in the initial dislocation structure (i.e., density/distribution of mobile dislocations) of each steel.

Work Hardening Rate as a Function of Strain

The work hardening rate, calculated for the entire stress-stress curves of samples A2-A29, B2-B18 and C2-C5 (in 0.5% strain increments), is shown in Figure 3. The work hardening rate for Steel B is clearly higher at low strain values compared with Steel A and Steel C. The difference in the work hardening rate observed in Steel B maybe partially attributed to a difference in the initial mobile dislocation density/distribution. With the application of sufficient strain, the work hardening rates of all three steels converge.

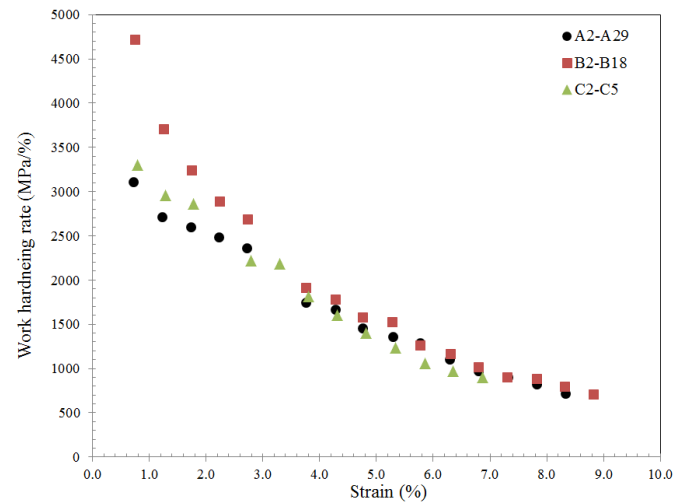


Figure 3 - Measured strain hardening rate for A-A29, B2-B18 and C2-C5

Tensile Testing – Strain Aged Samples

Tensile bars (see Figure 1) were either aged in the as-received condition (AR) or a pre-strain was applied (1.5% or 3.0%) followed by aging. The full aging procedure is described by Ma [5]. Following aging, the samples were tested in tension and the change in yield stress ($\Delta\sigma_y$) (relative to the as-received samples) and the Y/TS were measured. For the pre-stained samples, the value of $\Delta\sigma_y$ was determined based on the maximum stress incurred during pre-straining.

Table 3 lists the aging conditions and tensile test results for pipe Sample A. Table 4 and Table 5 tabulate the aging conditions and tensile results for Steel B and Steel C, respectively. The samples designated with a suffix "L" indicate a longitudinal tensile strip.

Table 3 – Strain Aging Conditions and results for Pipe A

Sample	T (°C)	Time (min)	Pre (%)	$\Delta\sigma_y$ (MPa)	Y/TS
A2-A12	175	25	1.5	66	1.0
A2-A13	175	5	1.5	55	0.98
A2-A28	175	15	A.R.	59	0.94
A2-A32	175	15	1.5	70	0.99
A2-A1	215	5	1.5	82	1.0
A2-A4	215	15	1.5	86	1.0
A2-A7	215	25	1.5	86	1.0
A2-A15	215	15	3.0	89	1.0
A2-A20	215	5	3.0	68	1.0
A2-A22	215	25	A.R.	65	0.94
A2-A24	215	25	3.0	89	1.0
A2-A26	215	15	A.R.	68	0.95
A2-A30	215	5	A.R.	61	0.95
A2-A31	215	15	1.5	80	1.0
A2-A2	255	5	1.5	89	1.0
A2-A6	255	15	1.5	95	1.0
A2-A19	255	15	3.0	75	1.0
A2-A21	255	15	A.R.	69	0.95
A2-L5-L	215	5	A.R.	24	0.87
A2-L8-L	255	5	A.R.	36	0.89
A2-L11-L	255	25	A.R.	40	0.90

Table 4 – Strain aging conditions and results for Pipe B

Sample	T (°C)	time (min)	Pre (%)	$\Delta\sigma_y$ (MPa)	Y/TS
B2-B4	175	5	1.5	59	0.95
B2-B11	175	15	3.0	62	0.99
B2-B19	175	15	A.R.	45	0.88
B2-B24	175	25	1.5	82	0.97
B2-B5	215	15	1.5	84	0.97
B2-B20	215	15	A.R.	59	0.89
B2-B17	255	25	A.R.	88	0.91
B2-B23	255	15	1.5	97	0.97
B2-M5A-L	215	5	A.R.	21	0.83
B2-36A-L	255	5	A.R.	10	0.84
B2-M11A-L	255	25	A.R.	67	0.96

Table 5 – Strain aging conditions and results for Pipe C

Sample	T (°C)	time (min)	Pre (%)	$\Delta\sigma_y$ (MPa)	Y/TS
C2-C7	175	15	1.5	59	0.96
C2-C9	215	15	A.R.	69	0.86
C2-C3	215	15	1.5	68	0.97
C2-C14	215	25	1.5	69	0.97
C2-C2	255	15	1.5	75	0.98
C2-C8	255	5	3.0	79	1.0
C2-N5A-L	215	5	A.R.	4	0.83
C2-N8A-L	255	5	A.R.	10	0.83
C2-N11A-L	255	25	A.R.	7	0.83

Microstructural Analysis – As Received

Optical and SEM images, taken from near the centerline at the 180° pipe position, are shown in Figures 4, 5 and 6 for Steels A, B and C, respectively. Metallographic samples taken near both the inner and outer surfaces of the pipe (not shown) exhibited similar microstructures to those shown in Figures 4, 5 and 6 though the grain size and volume fraction of phase(s)/microconstituents differed slightly [5]. EBSD analysis was also conducted on each steel but for brevity, the results are not included in this paper [5].

Steel A (Figure 4) exhibits primarily an acicular ferrite/bainitic structure with some polygonal ferrite and a small amount of pearlite. The pearlite in Steel A is outlined by the dashed circles. Steel B (Figure 5) exhibits a similar microstructure of acicular ferrite/bainite and polygonal ferrite but without the presence of pearlite. Steel C is comprised primarily of polygonal ferrite with a significant component of pearlite. In the optical image for Steel C (Figure 6), the dark areas are pearlite. The pearlite is circled in the SEM image for Steel C (Figure 6).

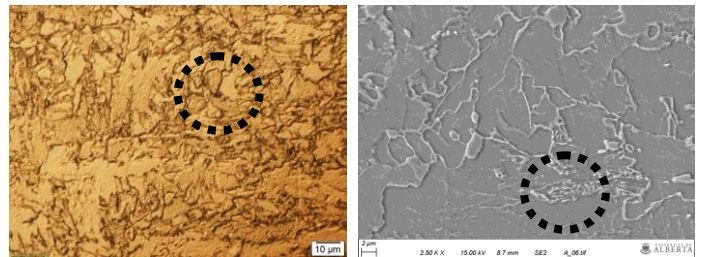


Figure 4 - Steel A - Left: Optical image. Right: SEM secondary electron (SE) image.

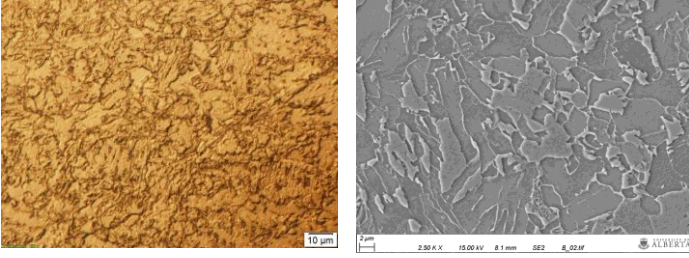


Figure 5 - Steel B - Left: Optical image. Right: SEM SE image.

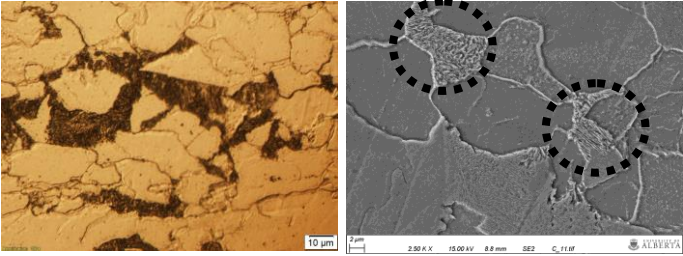


Figure 6 - Steel C - Left: Optical image. Right: SEM SE image.

For each steel, the phase fraction was measured using a grid overlay method (ASTM 112-13) and the grain size was measured using line intercept method (ASTM E562-11) from five (5) separate images taken near the centerline. The mean values of each are summarized in Table 6. The fraction of acicular ferrite/bainite and polygonal ferrite are relatively similar in both Steel A and Steel B. Conversely, Steel C shows 80% polygonal ferrite and 20% pearlite. The fraction of pearlite is above the amount that would be expected from the nominal carbon concentration of Steel C, however, carbon enrichment at the centerline due to segregation may account for the larger fraction of pearlite observed.

In addition, the average grain sizes of both Steel A and B are similar (8.5 µm compared with 7.8 µm), while Steel C has a significantly larger grain size (14.8 µm). This difference in grain size is observed qualitatively in Figures 4, 5 and 6.

Table 6 – Summary of average phase fractions and grain size

Steel	Acicular ferrite/bainite (%)	Polygonal ferrite (%)	Pearlite (%)	Grain Size (µm)
A	60	38	2	8.5
B	52	48	-	7.8
C	-	80	20	14.8

DISCUSSION

This section of the work analyzes the effect of time, temperature, steel type (microstructure and strain hardening rate) and pre-strain on the strain aging response ($\Delta\sigma_y$ and $\Delta(Y/TS)$) of the steels studied. Since carbon diffusion depends

on both time and temperature, a combined time/temperature diffusion parameter (DP) is used in the analysis. Based on the strain aging equation developed by Zhao et al. [6], the value of DP is calculated as:

$$DP = \left(\frac{D_T/T}{D_{175}/448} \right)^{2/3} \cdot t^{2/3} \quad (4)$$

where D_T is the diffusion coefficient for carbon at any aging temperature, D_{175} is the diffusion coefficient at 175°C and t is the time in seconds. The values of D_T and D_{175} were calculated using the Arrhenius diffusion equation ($D_0 = 6.2 \times 10^{-7} \text{ m}^2/\text{s}$ and $Q = 80 \text{ kJ}/(\text{mol}\cdot\text{K})$) at the aging temperature T (K) and at 175°C respectively.

Steel A

Figure 7 graphs the change in transverse (T) yields stress ($\Delta\sigma_y$) for the aged as-received (A.R.) and the aged pre-strained (1.5 and 3.0%) Steel A samples as a function of DP. Also included in Figure 7 is the data measured for aged longitudinal (L) samples taken from the same 180° location in Steel A. For low DP values, the A.R. steel and pre-strained steels exhibit similar behaviour; however, for larger DP values the AR steel levels off at a lower $\Delta\sigma_y$ value than either pre-strained sample.

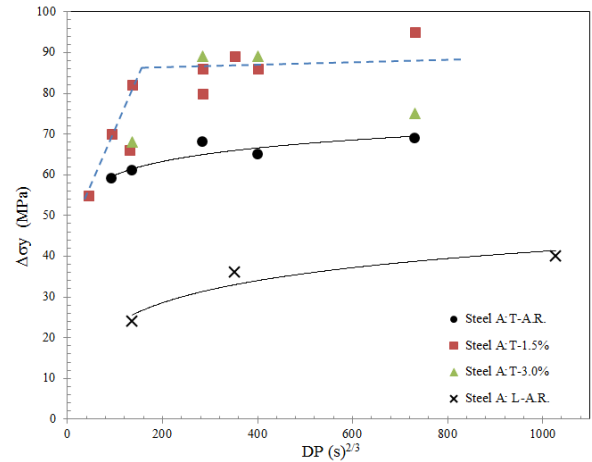


Figure 7 - Effect of aging and pre-strain on $\Delta\sigma_y$ for Steel A.

Figure 8 graphs the $\Delta(Y/TS)$ ratio for the aged AR and aged pre-strained (1.5 and 3.0%) transverse Steel A samples as a function of DP. After an initial rapid increase at low DP values, the value of $\Delta(Y/TS)$ reaches a maximum of 0.14 which corresponds to a $Y/TS = 1.0$ (essentially the yield stress is equivalent to the tensile strength). Both the as-received and longitudinal samples also reach a maximum value albeit of lower magnitude (≈ 0.085). The rapid attainment of both upper limits suggests the strain aging effect (i.e., carbon pinning of dislocations) occurs relatively rapidly in Steel A. Dashed lines have been added to Figure 8 to help illustrate the trends observed.

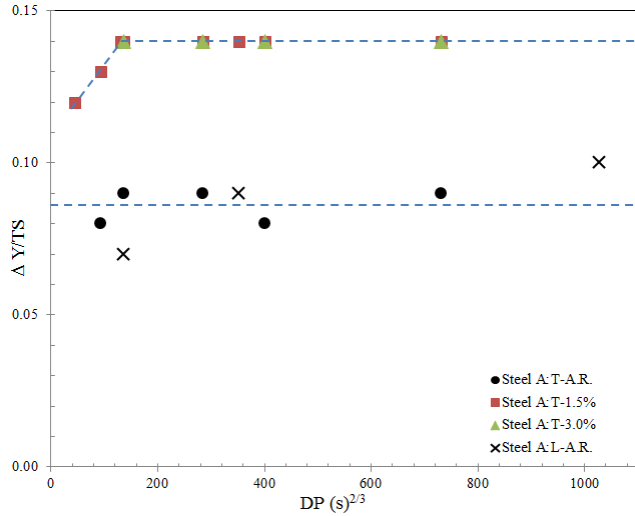


Figure 8 - Effect of aging and pre-strain + aging on $\Delta(Y/TS)$ for Steel A.

Comparison Between Steels A, B and C: As-received (AR)

Figure 9 graphs the change in $\Delta(Y/TS)$ for the aged as-received (A.R.) samples for all three steels. Dashed lines have been added to the figure to illustrate trends. Although the number of data points is limited, the $\Delta(Y/TS)$ values for Steel B are below those for Steel A (0.05 vs. ≈ 0.085) for smaller DP values. However, for larger DP values, the $\Delta(Y/TS)$ ratios for Steel B approach those of Steel A. This suggests that the distance carbon must diffuse (i.e., DP term) to “pin” a mobile dislocation is larger in Steel B than in Steel A.

Since the microstructures and grain sizes are similar for both Steel A and B (Table 6), the difference in behaviour may be related to the different initial work hardening rates of the two steels (≈ 5000 vs. ≈ 3000) as shown in Figure 3. This difference suggests that the two steels may have different initial mobile dislocation densities/distributions that may account for the differences in strain aging behaviour.

It is difficult to draw any conclusions for Steel C as only one sample (circled in Figure 9) was successfully tested. However, it appears that Steel C is less prone to the effects of strain aging than Steel A or Steel B, possibly stemming from its different microstructure, phase fraction and/or grain size.

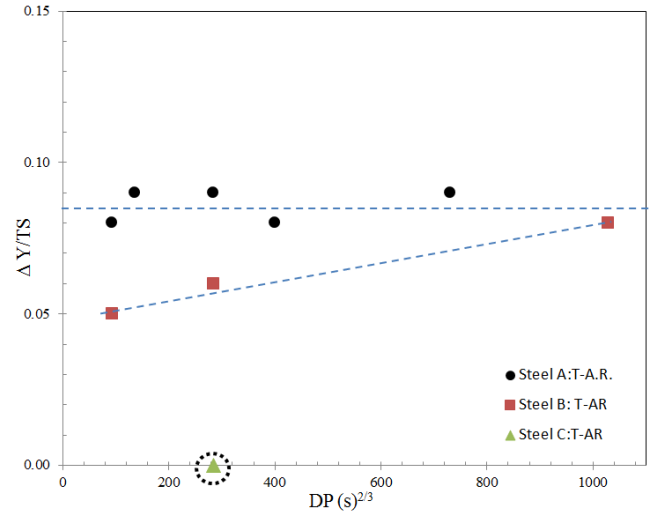


Figure 9 - Effect of aging on $\Delta(Y/TS)$ for AR samples from Steel A, Steel B and Steel C.

Comparison of Steel A, B and C: 1.5% Pre-strain Samples

Figure 10 graphs the change in $\Delta(Y/TS)$ for the aged 1.5% pre-strained samples for all three steels. Dashed lines have been added to the figure to illustrate trends. After pre-straining 1.5%, both Steel A and Steel B rapidly reach (for relatively small DP values) a strain aging condition in which the $\Delta(Y/TS)$ reaches a maximum value (i.e., the measured yield stress and tensile stress are equivalent).

The $\Delta(Y/TS)$ behaviour for Steel B after aging is different than the behaviour shown in Figure 9 for the as-received Steel B. However, it can be postulated that the rapid work hardening rate of aged Steel B results in a dislocation structure similar to that in Steel A after the application of a 1.5% pre-strain. This would account for the similar behaviour for the two steels after pre-straining.

Steel C, on the other hand, exhibits lower $\Delta(Y/TS)$ ratios at small DP values. However, as DP (i.e., the amount of carbon diffusion) increases, the aging effect becomes more significant in Steel C and the $\Delta(Y/TS)$ values approach those for Steel A and Steel B. As suggested earlier, the lower $\Delta(Y/TS)$ values at small DP and the gradual increase with increasing DP may be partially attributed to the greater distance the carbon must diffuse to “pin” mobile dislocations. Since the work hardening rate of Steel C is equivalent to that of Steel A, the difference may be partially attributed to the presence of a large fraction of polygonal ferrite in combination with a coarser (i.e., larger grain size) microstructure.

The application of 3.0% pre-strain prior to aging shows that the Y/TS ratio approaches a value of one (1) (Tables 3, 4 and 5) for all the steels. The convergence of the work hardening rate for all the steels at this strain (Figure 3) suggests that the mobile dislocation density/distribution becomes sufficiently similar such that the effect of aging on the properties is also similar.

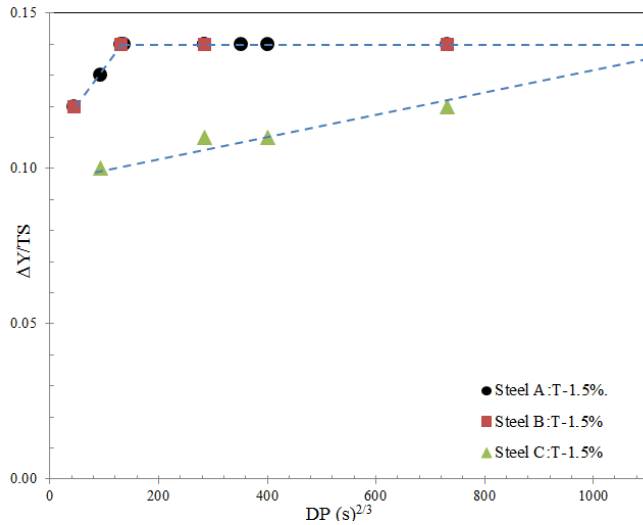


Figure 10 - Effect of aging on $\Delta(Y/TS)$ for the 1.5% pre-strained samples for Steel A, Steel B and Steel C.

CONCLUSIONS

The effect of strain aging on thick walled, X70, UOE pipeline steel was studied. The following conclusions are postulated.

- 1] For the test conditions conducted in this work, a microstructure consisting primarily of polygonal ferrite (and some pearlite) and a large grain size is less sensitive to the effects of strain aging.
- 2] For two X70 steels tested in this work, the steel with the higher initial rate of work hardening exhibited a smaller change in the Y/TS ratio at low diffusion times and/or temperatures.
- 3] For longer diffusion time and/or temperatures, the effect of strain aging on the $\Delta(Y/TS)$ converges for all three steels tested.
- 4] Further microstructure analysis on dislocation density is needed to support the postulation of the effect of initial work hardening rate on strain aging sensitivity.

NOMENCLATURE

σ_y	yield strength (0.5% offset method)
TS	tensile strength
Y/TS	yield strength over tensile strength
A.R.	as-received

ACKNOWLEDGMENTS

The authors would like to thank Laurie Collins and EVRAZ N.A. Inc for valuable input and financial support, Robert Lazor and TCPL for samples and financial support and NSERC for financial support.

REFERENCES

1. J.B. Wiskel, J. Ma, J. Valloton, D.G. Ivey and H. Henein: *Mat. Sci. Tech.*, A, Vol. 33, pp. 1319-1332, 2017.
2. A.W. Bowen and P.G. Partridge: *J. Phys. D*, Vol. 7, pp. 9691-978, 1974.
3. Y. Bergstrom: *Mat. Sci. Eng.*, Vol. 5, pp. 192-200, 1969/70.
4. J. B. Wiskel, M. Rieder and H. Henein: *Can. Met. Quar.*, vol. 43 (1), pp.125-136, 2004.
5. J. Ma, M. Sc. Thesis, University of Alberta, 2016, Canada.
6. J.Z. Zhao, A.K. De and B.C. De Cooman, "Kinetics of Cottrell atmosphere formation during strain aging of ultra-low carbon steels", *Mat. Lett.*, vol. 44, pp. 374-378, 2000.